NASA TECHNICAL MEMORANDUM

NASA TM X-52803

NASA TM X-52803

A SUB-MILLIPOUND MERCURY ELECTRON-BOMBARDMENT THRUSTER

by Paul D. Reader, Shigeo Nakanishi, Walter C. Lathem, and Bruce A. Banks
Lewis Research Center
Cleveland, Ohio

TECHNICAL PAPER proposed for presentation at
Sixth Propulsion Joint Specialists Conference sponsored by
the American Institute of Aeronautics and Astronautics
San Diego, California, June 15-19, 1970

A SUB-MILLIPOUND MERCURY ELECTRON-BOMBARDMENT THRUSTER

by Paul D. Reader, Shigeo Nakanishi, Walter C. Lathem, and Bruce A. Banks

Lewis Research Center
Cleveland, Ohio

TECHNICAL PAPER proposed for presentation at

Sixth Propulsion Joint Specialists Conference sponsored by
the American Institute of Aeronautics and Astronautics
San Diego, California, June 15-19, 1970

NATIONAL AERONAUTICS AND SPACE ADMINISTRATION

A SUB-MILLIPOUND MERCURY ELECTRON-BOMBARDMENT THRUSTER

Paul D. Reader, Shigeo Nakanishi, Walter C. Lathem, and Bruce A. Banks

Lewis Research Center
National Aeronautics and Space Administration
Cleveland, Ohio

E-5678

Abstract

Several similar 5 cm diameter electron bombardment ion thrusters were investigated. A series of tests used to improve the performance of the thruster components are discussed. Cathode pole piece and baffle position and geometry significantly influence ion chamber performance and are used to tailor the discharge characteristics to obtain desired operational modes. Both chamber and neutralizer emitters are enclosed hollow cathode types. The chamber cathode operates on the total flow through the discharge chamber. The neutralizer cathode has been operated successfully at mercury flow rates below 2 mA of equivalent flow while coupled to an operating thruster beam. All thruster tests were conducted with single, glass coated grids. Tests of glass-coated grids designed to provide single and multiple axis electrostatic thrust vectoring are also discussed. A thruster system design resulting from the above component tests is described. Overall thruster efficiencies of 20 percent at a specific impulse of 1800 sec have been demonstrated at a thrust level of 0.36 mlb.

Introduction

Spacecraft in operation today have demonstrated impressive gains in reliability and useful life over those launched during the early 60's. Future orbiting spacecraft with design lifetimes of several years place severe requirements on attitude control and station keeping subsystems. The long life and high value of specific impulse available from low thrust, electrostatic thruster systems make them increasingly competitive for these functions. Thrust levels in the submillipound range, for example, are of particular interest for spacecraft in the 1000 to 2000 lb class.[1,2]

This paper presents the results of component tests of several 5-cm-diameter mercury electron-bombardment ion thrusters. Ion chamber and magnetic field variations are described. Results with enclosed hollow cathodes used for both the main chamber and the neutralizer emitters are presented and compared with open hollow cathodes of the type flown on Space Electric Rocket Test II (SERT II).[3] All thruster tests were conducted with single, glass-coated accelerator grids.[4] Accelerator grid fabrication techniques and several grid designs (including vectorable grids) are described. Finally, a thruster system design resulting from these component tests is detailed. Some spacecraft applications possible with this thruster system are then considered.

The vacuum facility used for this investigation was 4.5 m long by 1.5 m in diameter. The thruster test chamber was connected to the facility through a 0.3 m gate valve. A stainless steel tank-divider limited the ion beam length to 2 m. The facility was maintained at 10^{-6} torr during thruster operation. Details on the facility are found in Ref. 5.

Discharge Chamber

A cross section of the thruster discharge chamber used for research tests is shown in Fig. 1. The length of the discharge chamber was changed by substituting different length chamber shell and anode sections. Five different lengths were tested.

The conical cathode pole piece has screen covered holes in its sides to allow mercury from the cathode to flow radially into the discharge chamber. The diameter and location of the downstream end of the cathode pole piece were scaled from SERT II. The conical shape was necessary to provide cathode clearance. The baffle was kept at the plane of the downstream surface of the conical pole piece for all tests but the shape was varied. Full cover baffles with various hole sizes in the center and centrally located disc baffles of different diameters were tested. The discs were suspended by 3 wires, 120^{o} apart attached to the pole piece. The magnetic field strength was varied by changing the number of rod magnets.

In addition to these changes, ranges of neutral flow rates and voltages were tested. Precision, 0.5 mm bore glass tubing was used as propellant reservoirs for the research runs to allow accurate mercury flow rate measurements.

Fig. 2 shows the effect of net accelerating voltage variations on discharge chamber losses per beam ion (eV/ion) for three chamber lengths studied. The glass coated grid used for these tests is described in a later section.

The effect of increasing net accelerating voltage is a marked improvement in discharge efficiency (lower eV/ion) for the three chamber lengths shown. The discharge losses decreased by more than a factor of two as the chamber was shortened from 6.67 cm to 4.76 cm. The 4.76 cm long chamber was best and operated with primary discharge losses of 110 eV/ion at a net accelerating potential of 650 V.

Individual changes in magnetic field, pole piece baffle configuration and propellant utilization efficiency were also made, however, the chamber length was found to be the dominant factor in improving thruster performance as shown in Fig. 3. The curves are lines of constant discharge energy loss per beam ion produced. They are shown to allow discharge efficiency comparisons between configurations having operating points at different discharge currents and voltages. The data

points associated with a particular chamber length fall roughly along lines of constant discharge energy loss per beam ion. The data scatter in each case is due mainly to the effects of baffle shape, magnetic field strength and propellant utilization efficiency. Baffles with central holes and high magnetic field strengths increased discharge voltage while disc baffles and moderate field strengths lower the voltage. Operation at higher propellant utilization efficiency required lower propellant flow rates at a constant beam current resulting in a lower density, higher voltage discharge characteristic.

In the range of discharge voltage between 20 and 40 V the discharge performance improved with decreasing chamber length for a number of other parametric changes. The 4.76 cm long chamber operated at discharge losses below 200 eV/ion. A 3.75 cm length chamber was briefly tested and exhibited very unstable operation with higher discharge losses. Further optimization tests are being conducted on magnetic field and baffle configurations using the 4.76 cm long chamber.

It should be noted that at the 110 eV/ion point previously mentioned only 3.4 W were consumed in the primary chamber discharge but 7 W (or about 230 eV/ion) were lost in the cathode keeper discharge. Thus, for small thrusters several power losses become of the same magnitude as ionization losses. The ionization losses are therefore more representative of thruster performance for larger thrusters than for smaller thrusters.

Cathodes

Main Cathodes

The two types of hollow cathodes used in this program are shown in Fig. 4. The SERT II type, or open hollow cathode, is shown in Fig. 4(a). Mercury vapor flows into a 0.32 cm diameter tantalum tube closed at one end except for a small aperture in a two percent thoriated tungsten tip. An insert coated with barium carbonate aids the initiation of a cathode discharge and generally improves cathode emission. The cathode tip is heated electrically by an encapsulated tungsten-rhenium heater element. The cathode discharge is started by heating the cathode tip and applying about 300 V potential between the cathode and the keeper. The keeper is a 4.8 mm inside diameter ring fabricated of 1.52 mm wire. The ring is 1.5 mm downstream of the cathode orifice.

A cutaway sketch of the enclosed cathode type is shown in Fig. 4(b). The changes made to the open cathode were done in an attempt to minimize discharge coupling voltage effects and radiated heat losses. Also of equal importance is the fact that the integrated construction provides positive spacing and alinement of the keeper electrode. The tantalum keeper cap was 0.25 mm thick with a 3.2 mm diameter aperture. The keeper was positioned 1.5 mm from the cathode aperture by means of a ceramic tube over the cathode body. A ceramic retaining collar cemented to the cathode body held the keeper and tube in the proper relative positions. Disassembly was accomplished easily by removing the keeper lead retaining wire.

Fig. 5 shows a comparison of data taken with the open and enclosed cathodes at the same thruster operating conditions. The open cathode operation bands are shown shaded and the enclosed cathode data are shown as symboled curves.

With the open cathode the chamber discharge current and voltage and cathode keeper voltage were nearly constant for keeper currents between 0.2 and 0.5 A as the cathode heater power was dropped from 16 to 5 and finally 0 W. One variation from this condition was an instability which developed at keeper currents below 0.25 A when the open cathode was at zero heater power. Enclosed cathode operation at similar powers showed a wider range of keeper voltage, discharge voltage, and discharge current.

From these data it was concluded that either hollow cathode could satisfy the main chamber cathode requirements. Cathode heat losses can be reduced while maintaining the necessary cathode temperature by using improved shielding and insulating techniques. The enclosed cathode demonstrated greater stability over a wider range of discharge chamber variables than the open cathode and is of greater interest because of its structural integrity.

Neutralizer. - The operating requirements for the neutralizer are low neutral propellant flow, minimum heating power, and low beam coupling voltage. Enclosed and open cathodes, identical in design to those described in the previous section (Fig. 4), were tested for use as neutralizers.

The effect of neutralizer flow upon keeper voltage of the open and enclosed configurations tested with a simulated beam is shown in Fig. 6. The data from Ref. 6 for the SERT II neutralizer operating with a thruster system is also shown on the figure as a dashed curve. The open and enclosed cathodes were tested by starting a discharge to a collector anode to simulate thruster operation. Both the open keeper and the SERT II configurations were operated with heater power while the enclosed keeper was not.

Fig. 6 shows that with the open keeper, the keeper voltage began to rise sharply at a flow rate of about 8 mA equivalent neutral flow. The keeper discharge ceased to operate below about 6 mA of neutral flow. The differences in the open keeper and SERT II keeper discharge characteristics may be due to the difference in heater power levels.

The neutralizer cathode with the enclosed keeper was operated with no heater power, a stringent condition which should give less optimistic results than operation with heater power. As shown in Fig. 6, the keeper discharge operated successfully down to neutral flows of less than 2 mA. On the basis of required neutral flow, the enclosed keeper hollow cathode is superior to the open cathode for neutralizer operation on a 5 cm thruster.

A smaller diameter version of the enclosed hollow cathode was fabricated of 0.203 cm outside diameter tantalum tube and tested on a 5 cm thruster. All other cathode design features were essentially unchanged. Preliminary results are shown in Fig. 7. At zero heater power and 0.35 a keeper current the keeper voltage was approximately equal to that obtained for simulated beam operation (see Fig. 6). This supports the viewpoint that simulated beam tests of neutralizers are valid and also suggests that a reduction in cathode outside diameter had no affect on performance. With the application of heater power, lower neutralizer keeper voltages were possible at a given value of keeper current.

The variation in thruster floating potential with neutralizer keeper current for the four levels of heater power is shown in Fig. 7(b). As noted above, the trend observable in the keeper voltage was reflected in the floating potential.

Satisfactory neutralization has been obtained with an enclosed hollow cathode at neutral flow rates as low as 2.25 mA. Sufficient electron emission for neutralization at low heater power appears feasible with further improvements in thermal design.

Accelerator Grid Fabrication and Performance

Both composite and double grid systems have been tested on 5 cm diameter thrusters.[7,8] The results of Ref. 8 showed that the discharge power loss was reduced by about one half when a double grid system was replaced by a glass coated, or composite grid. All of the grid system tests discussed in this paper were conducted with composite grids.

Non-Vectorable Grids

A photograph of a portion of the grid used for the discharge chamber studies is shown in Fig. 8. The glass coated side (Fig. 8(a)) was covered by 0.57 mm thick Corning 7052. Fig. 8(b) shows the downstream face of the coated 0.38 mm thick punched molybdenum sheet having a hexagonal array of 1.91 mm diameter holes. The glass coating also covers the hole walls as seen in Fig. 8(b) so that the actual coated hole inside diameter is 1.38 mm. The grid was fabricated according to the process described in Ref. 4.

A molybdenum button rake system was used to obtain current density profile measurements with this grid. Fifteen, 1.27 cm diameter molybdenum discs were spaced along the 51 cm rake. The rake was located 58.4 cm downstream of the accelerator grid and traversed 40.6 cm across the ion beam.

Fig. 9 shows a block diagram of the ion beam profile measuring and processing equipment. This equipment is described in detail in Ref. 9. The currents measured at the molybdenum buttons was processed on a digital computer and the results stored on magnetic tape. Further computer processing yielded microfilm plots showing two dimensional contour maps of equal current density, coordinates of the centroid of the distribution and an integrated value of beam current.

Fig. 10 shows a typical contour plot made from probe rake measurements. The dashed contour is a 0.1 maximum current density contour taken with the same grid operating at a lower accelerating voltage. The beam divergence half-angle represented by the dashed curve is 20^{o}.

Over 200 hours of testing have been accomplished with the grid used to make these measurements without visible deterioration to the grid. Accelerator drain currents have been less than one percent of the beam current.

Vectorable Grids

Thrust vectoring systems which operate without the use of moving parts are desirable. Several electrostatic thrust vectoring grid designs were investigated and will be briefly discussed.

A two dimensional aperture grid consisting of parallel bars of molybdenum was designed to provide vectoring capability in two orthogonal directions. A cross section view of a typical element set is shown in Fig. 11 and the coated grid is shown in Fig. 12. The grid was fabricated by electric discharge machining. The grid geometry was designed so as to provide support and positive separation of elements during fusing of the glass to the grid. This grid was repeatedly slurry sprayed and fired with Corning 7052 glass until a thickness of approximately 0.6 mm was achieved. The final firing of the grid consisted of fusing a molybdenum ring to the periphery of the grid. This ring provides both additional mechanical support to the grid and electrically isolated mounting.

Thin slots in the molybdenum periphery shown in Fig. 12 were electrochemically machined away to provide four electrically isolated quadrants and one common set of conductor elements that interlace each of the four quadrants. The quadrants were electrically connected to provide deflection in the same direction from diametrically opposing quadrants. Preliminary tests of this grid indicated that the interlacing combs of elements could support accelerator potentials differences of over 100 V. However, after only a few minutes of thruster operation an accumulation of back-sputtered metal on the downstream surface of glass between the conductors caused shorting of the interlacing combs. The rapid buildup of conducting sputtered metal which caused shorting of the grid electrodes appears to be a facility testing problem due to back sputtered material from vacuum facility walls and target. Sputtered material from the thruster ground screen, neutralizer or from the downstream face of the grid itself may also have contributed to the problem, but can be overcome by appropriate design. Close inspection of the upstream face of the grid showed a very thin glass coating covering two areas near the grid center. These areas suffered electrical breakdown and direct ion impingement while the grid was operating on the thruster. Fig. 13 is a beam current density contour map taken of the quadrant grid operating with all elements at the same potential. The four current density peaks shown in Fig. 13 result from the overlapping of the beams from

each quadrant. (A two-dimensional aperture produces a fan beam with the greater spread normal to the long aperture dimension.)

One method to eliminate the local thin spots on grid glass coating is to make the single conductor elements much wider so that they appear similar to the double conductor elements. A grid of this design, coated with Corning 1723 glass was fabricated and tested. This grid was capable of sustaining high voltage, and higher beam currents (35 mA) were possible, but again back sputtered material from the facility resulted in shorting of the parallel conductors.

In another approach to a vectorable grid design, a method of fusing two molybdenum wires to Corning 7052 cane was investigated. Operationally this concept is similar to the previous grid, except that vectoring would only be accomplished in one direction. Fabrication consisted of heating two 0.38 mm molybdenum wires that were kept in tension. Lengths of 3.3 mm diameter cane were placed on the two taut wires. By heating to various temperatures in a nitrogen environment it was possible to determine how much the wires would inbed themselves in the glass. Fig. 14 shows a plot of the ratio of penetration depth into the glass cane to the wire diameter for various temperatures for one hour in a preheated oven. Slow cooling of these composite elements was necessary to prevent cracking. Fig. 15 is a photograph of a completed grid made from 15 elements fired at 904° C. Even though firing at this temperature resulted in a penetration depth about equal to the wire diameter there still remained a strip of exposed molybdenum approximately 0.25 mm wide on each wire. The center-to-center spacing between each cane was 5 mm. The ion extraction gap was 3 mm. Closer spacing was not possible because of a bulging at the ends of the glass cane. As a result, during testing, electron backstreaming occurred even at highly negative accelerator grid potentials. An improved design that also shadow shields the downstream surfaces from sputtered material is shown in Fig. 16. Fabrication techniques for this design are currently being investigated.

Another concept for thrust vectoring using multiple electrodes bonded to a laminated insulator which contains multiple axisymmetric apertures is shown in Fig. 17. The grid consists of two 0.81 mm thick glass sheets with conducting silver paint strips on each side of a rectangular array of holes. The holes were glass bead blasted through the glass using a drilled metal template. The silver conductor strips were painted on both sides of the downstream glass sheet. The upstream glass sheet shielded the downstream sheet from the ions in the discharge plasma.

A thruster test of this grid resulted in considerable electron backstreaming because of the large hole diameters. A contour plot of the beam taken with all conductors at the same potential is shown in Fig. 18. The profile is of interest because of the relatively flat, rectangular shaped contours near the peak values. The test showed that smaller accelerator apertures and more substantial conductors are required.

Thruster System

The efficient and smooth operating component configurations were assembled for thruster system tests. Table I contains five columns of thruster system characteristics. The first three columns are data taken during thruster system tests. All data were taken with the same thruster at the same time with the exception of the neutralizer performance. The neutralizer data were taken on another thruster operating at the same beam current, extraction voltage, and propellant utilization efficiency as the thruster data in the respective column. The final two columns represent projected performance predictions. Hardware to evaluate these predictions is presently being fabricated. The major changes being made are to weld cathodes and vaporizers into single assemblies and to incorporate additional radiation shielding to minimize component heat losses. The projected columns list points at about 1800 and 2400 sec specific impulse. Reduced component size and improved discharge and extraction performance are longer range goals.

Thruster data from Table I were used to size the propellant tankage for a rather arbitrarily defined five year North-South station keeping requirement aboard a 1500 lb synchronous satellite. Incorporating all of the component characteristics into the system resulted in the design shown in the cutaway view of Fig. 19.

A positive expulsion single tank feed system operating at spacecraft potential supplies mercury to both the main and neutralizer cathodes. The nitrogen gas pressure in the volume surrounding the propellant tank deflects a hemispherical rubber bladder to keep liquid mercury in the main and neutralizer feed lines. Heated porous tungsten discs located in the lines vaporize the mercury at a controlled rate. Vapor from the main vaporizer flows through a high voltage isolator and into the main cathode. The electrical isolator separates feed system components at spacecraft potential from those at thruster net accelerating potential. The mass of the thruster system shown in Fig. 19 is expected to be less than 2.1 kg. The tank holds 6.2 kg of mercury. Total impulses available with this propellant load range from 24 000 lb-sec at the demonstrated conditions of column 2, table I, to 33 000 lb-sec at the projected conditions of column 5.

Although attitude control and station keeping requirements for 1000 to 2000 lb synchronous spacecraft are the most immediate applications of the submillipound ion thruster, other uses are possible. The high total impulse capability on long duration missions can also be used to provide inertia wheel or control moment gyro momentum dump systems for high pointing accuracy spacecraft such as orbiting or interplanetary observatory vehicles. The same high impulse capability and under 100 W power requirement may be of use as trajectory shaping propulsion on small, RTG powered outer planet probes and orbiters.

Concluding Remarks

A series of evaluation tests have been performed on

components of 5 cm diameter electron bombardment ion thrusters. Power-to-thrust ratios of 190 W/mlb have been obtained at a specific impulse of 1800 sec. The best overall efficiency was 20 percent at a specific impulse of 1800 sec. It is estimated that simple thermal design cleanup of cathode and vaporizer units will allow operation at 140 W/mlb and 29 percent overall efficiency at 1800 sec. Preliminary testing with several electrostatic thrust vectoring concepts has resulted in the identification of some critical operational problems without a successful demonstration of beam vectoring. No fundamental barriers have been identified, however, and the investigation of electrostatic vectoring is proceeding.

References

1. Boucher, R. A., "Electrical Propulsion for Control of Stationary Satellites," Journal of Spacecraft and Rockets, Vol. 1, No. 2, Mar.-Apr. 1964, pp. 164-169.

2. Duck, K. I., Bartlett, R. O., and Sullivan, R. J., "Evaluation of an Ion Propulsion System for a Synchronous Spacecraft Mission," Paper 67-720, Sept. 1967, AIAA, New York, N. Y.

3. Rawlin, V. K. and Kerslake, W. R., "SERT II: Durability of the Hollow Cathode and Future Applications of Hollow Cathodes," Journal of Spacecraft and Rockets, Vol. 7, No. 1, Jan. 1970, pp. 14-20.

4. Banks, B. A., "A Fabrication Process for Glass Coated Electron-Bombardment Ion Thruster Grids," TN D-5320, 1969, NASA, Cleveland, Ohio.

5. Keller, T. A., "NASA Electric Rocket Test Facilities," Seventh National Symposium on Vacuum Technology Transactions, C. R. Meisner, Ed., Pergamon Press, New York, 1961, pp. 161-167.

6. Byers, D. C. and Staggs, J. F., "SERT II: Thruster System Ground Testing Performance," Journal of Spacecraft and Rockets, Vol. 7, No. 1, Jan. 1970, pp. 7-14.

7. Margosian, P. M., "Preliminary Tests of Insulated Accelerator Grids for Electron Bombardment Thrustor," TM X-1342, 1967, NASA, Cleveland, Ohio.

8. Nakanishi, S., Richley, E. A., and Banks, B. A., "High-Perveance Accelerator Grids for Low-Voltage Kaufman Thrustors," Journal of Spacecraft and Rockets, Vol. 5, No. 3, Mar. 1968, pp. 356-358.

9. Lathem, W. C. and Staggs, J. F., "Divergent-Flow Contact-Ionization Electrostatic Thrustor for Satellite Attitude Control and Station Keeping," TN D-4420, 1968, NASA, Cleveland, Ohio.

	Data			Projection	
	1	2	3	4	5
Beam power, W	13.5	19.5	19.5	19.5	30.0
Accel. drain, W	.14	.20	.18	.2	.45
Discharge, W	12.4	7.8	3.4	6.8	6.6
Cathode					
Keeper, W	4.6	4.6	7.0	3.5	3.5
Heater, W	15.0	15.0	16.4	7.0	7.0
Vaporizer, W	4.6	4.6	7.6	3.0	3.0
Neutralizer					
Keeper, W	3.36	3.36	3.36	3.0	3.0
Heater, W	9.4	9.4	9.4	5.0	5.0
Vaporizer, W	3.38	3.38	3.38	2.5	2.5
Total, W	66.4	67.8	70.2	50.5	61.1
Power efficiency	20.4	28.7	28.0	38.6	49.2
Prop. Util. Eff.	70	70	72	75	75
Overall Eff.	14.2	20.1	20	29	37
Beam current, mA	30	30	30	32	32
Thrust, mlb	.30	.36	.36	.36	.44
Isp, sec	1500	1800	1800	1800	2400
P/T, W/mlb	221	188	194	140	138

TABLE 1 5 CM THRUSTER SYSTEM PERFORMANCE

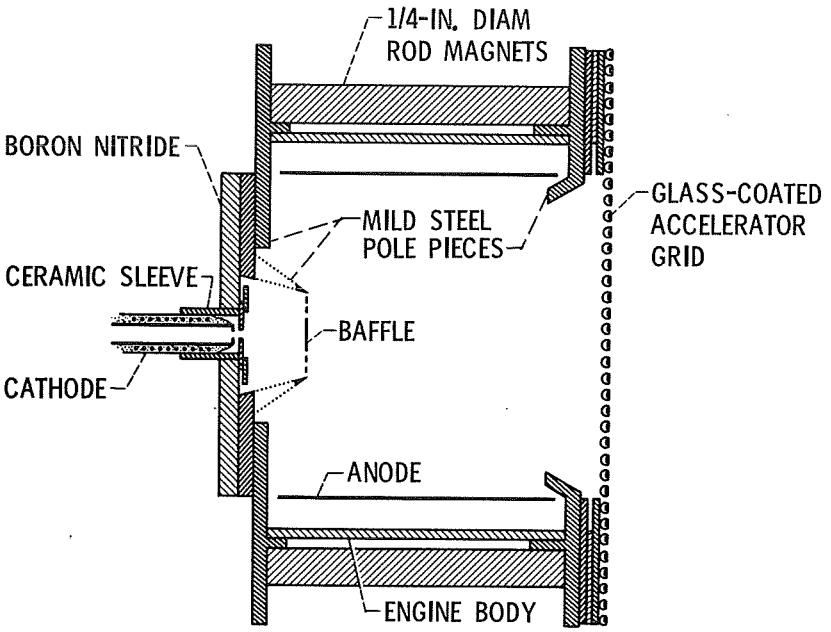

Figure 1. - Cross section of 5-cm diameter thruster discharge chamber.

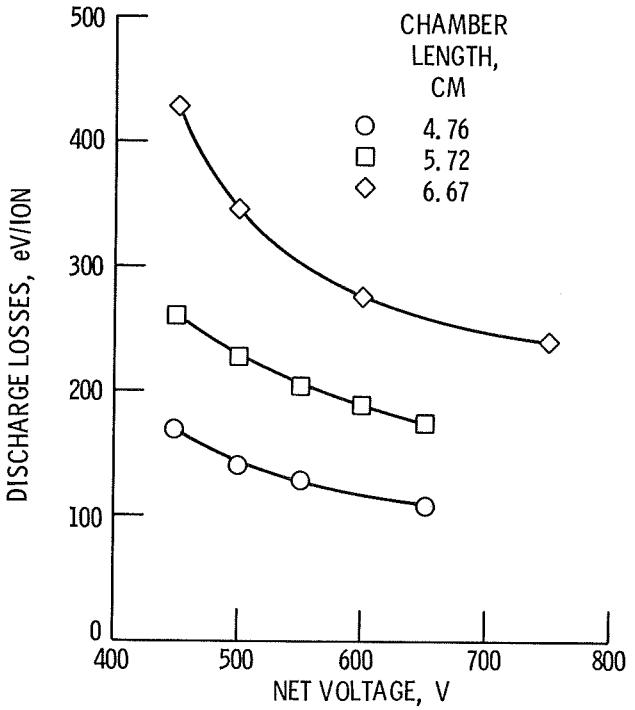

Figure 2. - Effect of net accelerating voltage on discharge chamber losses for three ion chamber lengths with 34 - 36 volt discharges, 70 percent propellant utilization efficiency, and 30 mA beam current.

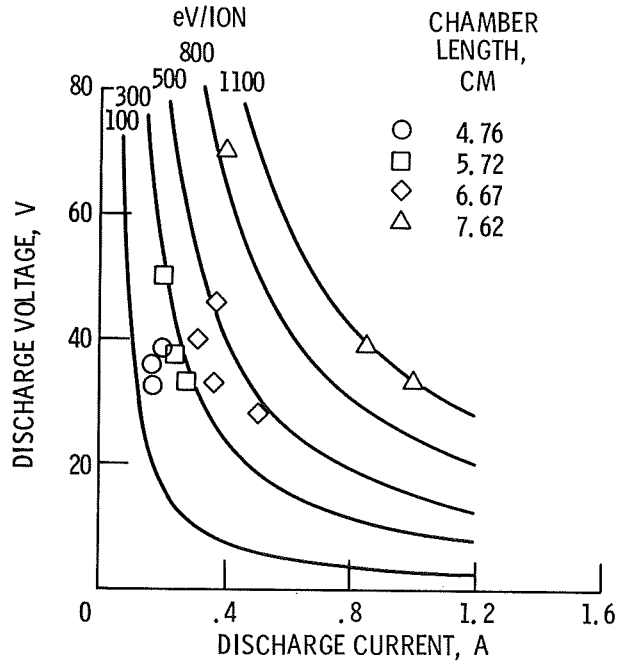

Figure 3. - Discharge chamber current voltage relationship for four chamber lengths. Beam current was 30 mA, net accelerating voltage 450 volts and total extraction voltage 675 volts.

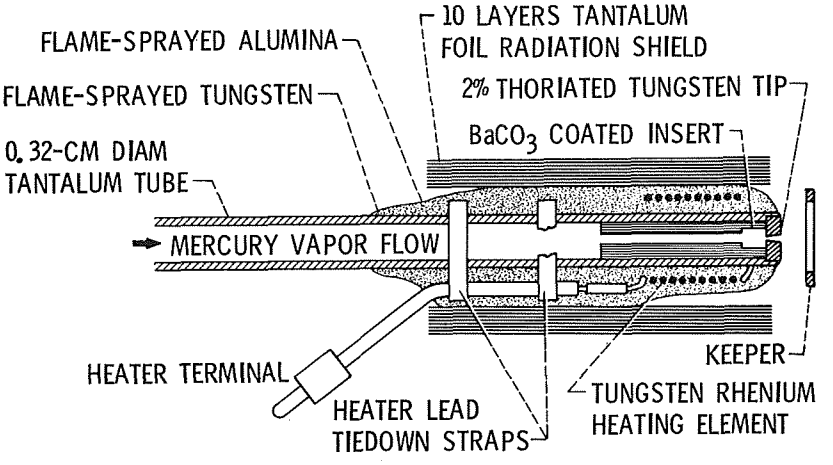

(A) OPEN CATHODE.

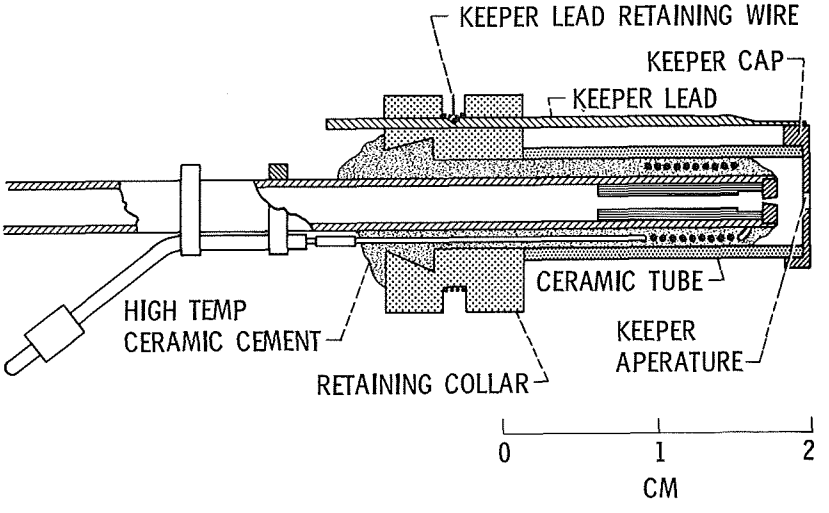

(B) ENCLOSED CATHODE.

Figure 4. - Comparison of open (SERT II) and enclosed hollow cathodes configuration.

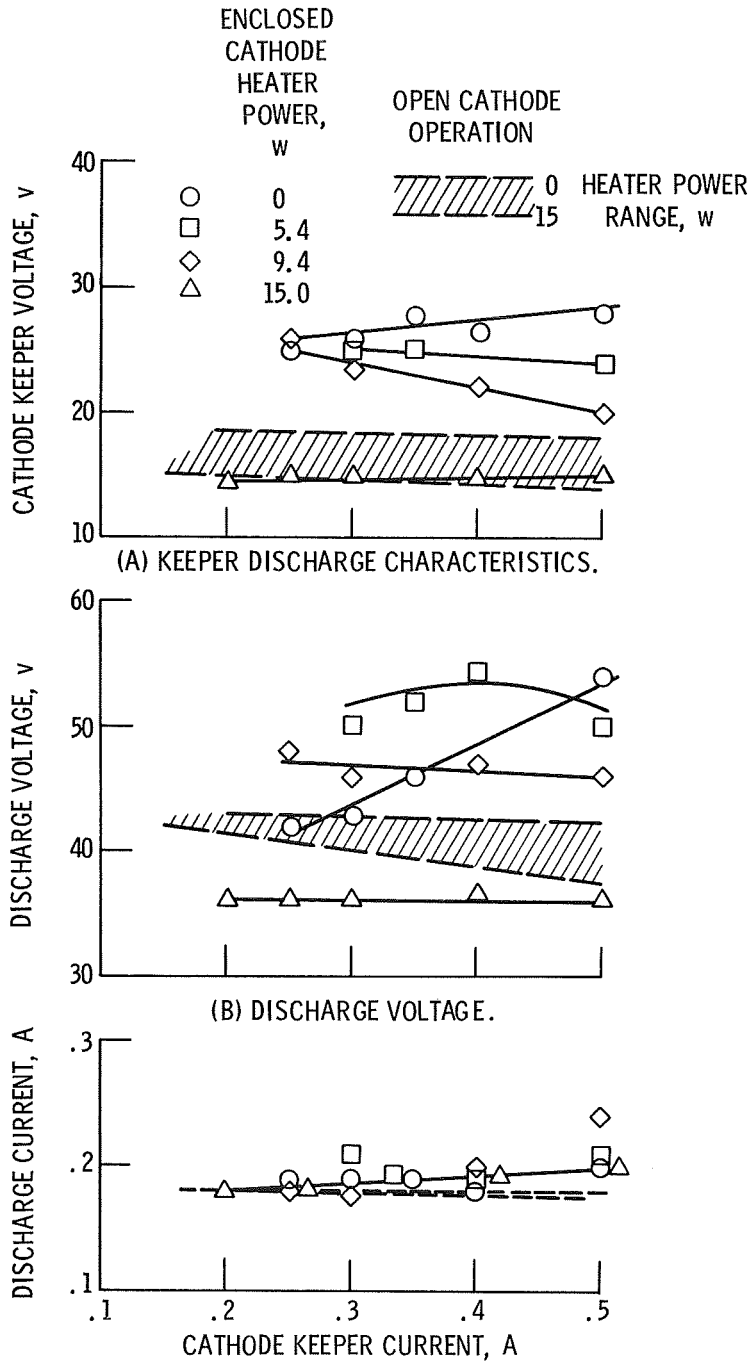

Figure 5. - Ion chamber and cathode characteristics with net accelerator voltage 650 V, propellant utilization efficiency of 68 percent, and propellant flow rate of 42 mA.

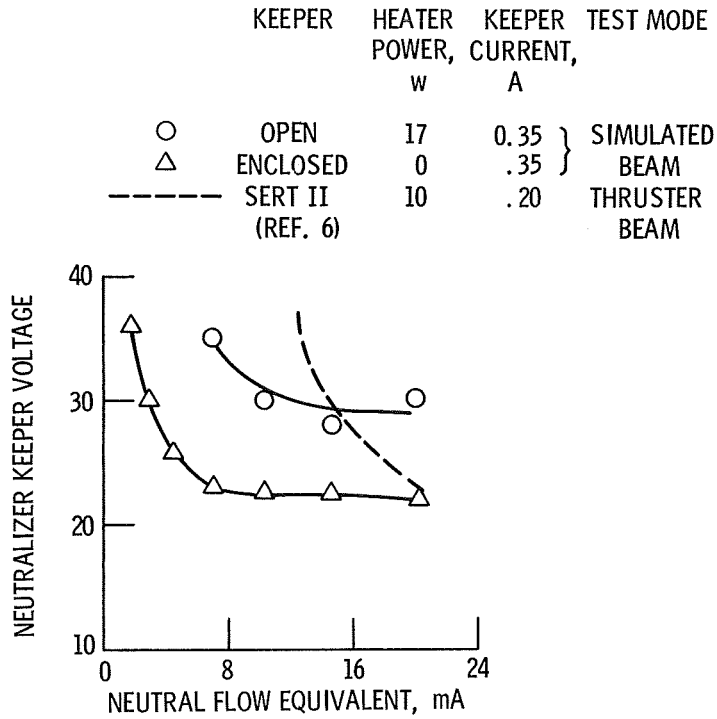

Figure 6. - Keeper discharge characteristics of neutralizers.

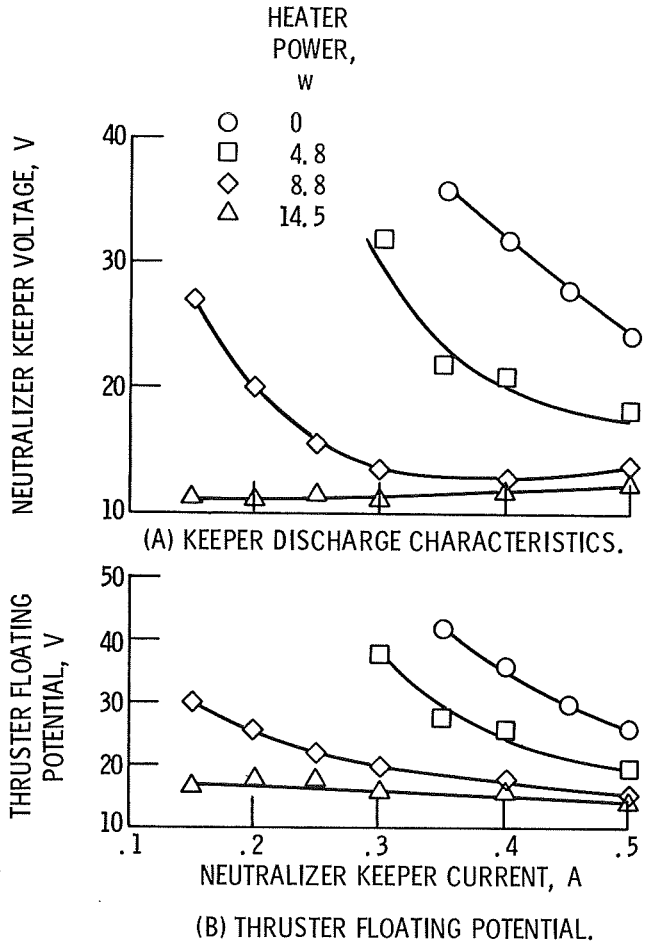

Figure 7. - Neutralizer discharge characteristics of reduced size (2/3 SERT II diameter) enclosed cathode with ion beam current of 0.030 A, net accelerating voltage of 650 V and neutralizer flow rate of 2.25 mA.

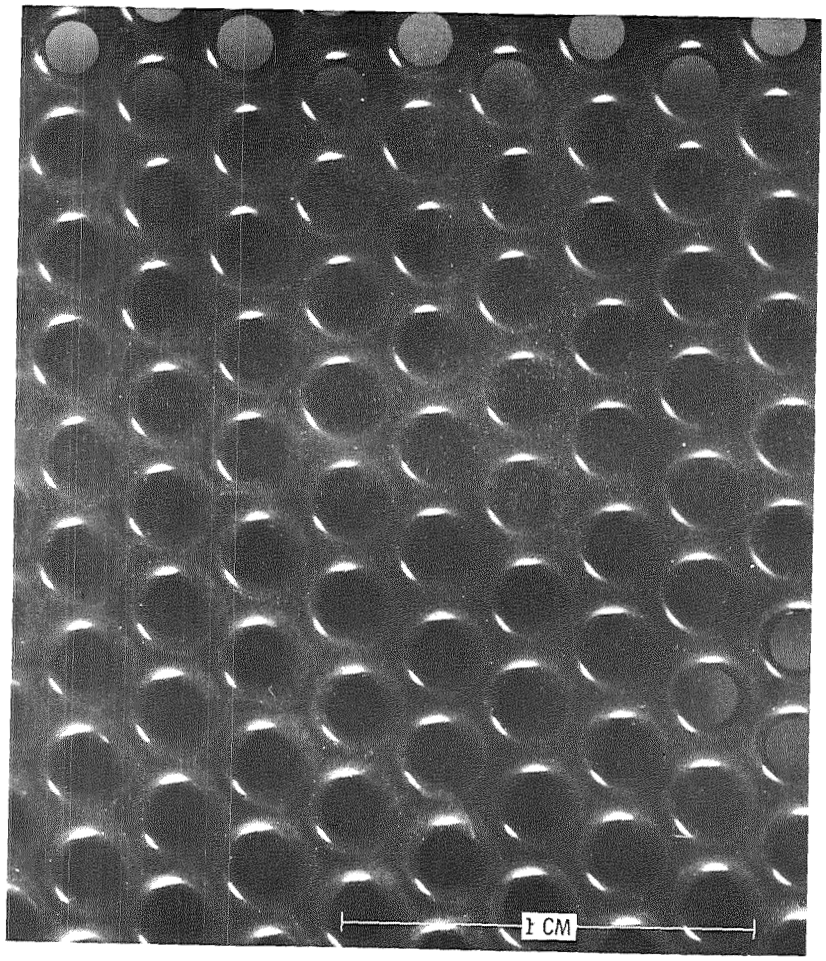

(a) Glass coated side.

Figure 8. - Central area of glass coated grid used for discharge chamber studies after about 100 hours of operation.

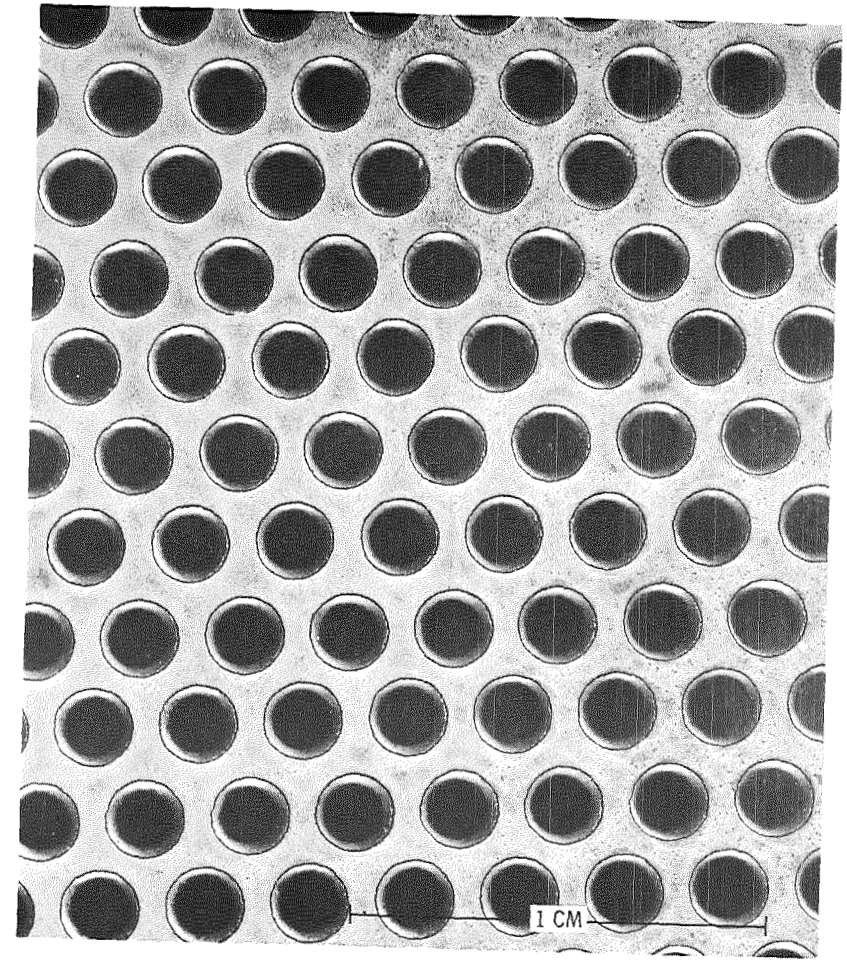

(b) Uncoated side.

Figure 8. - Concluded.

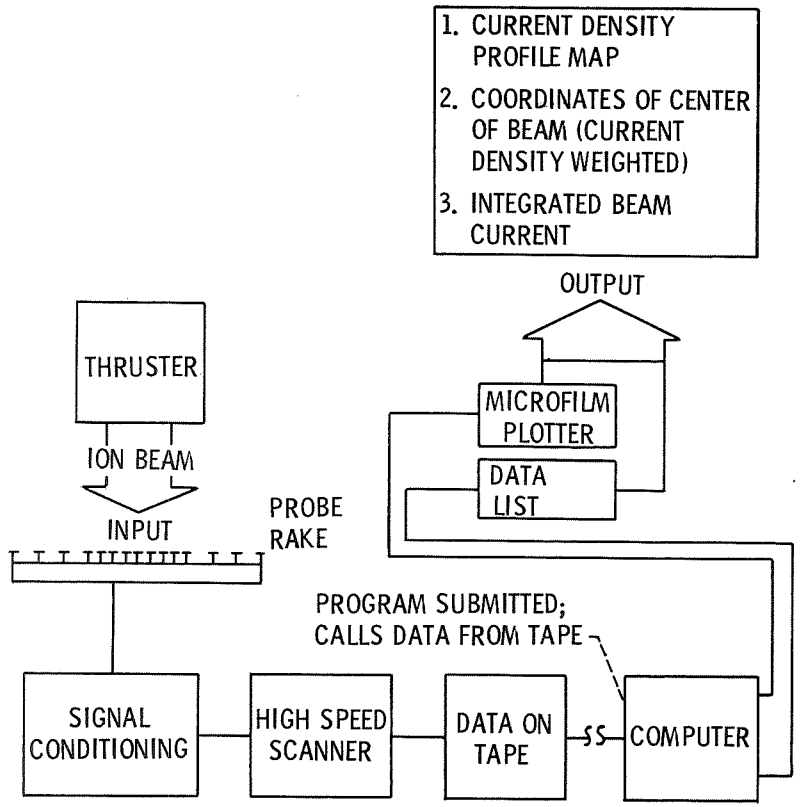

Figure 9. - Block diagram of system used to analyze the ion beam.

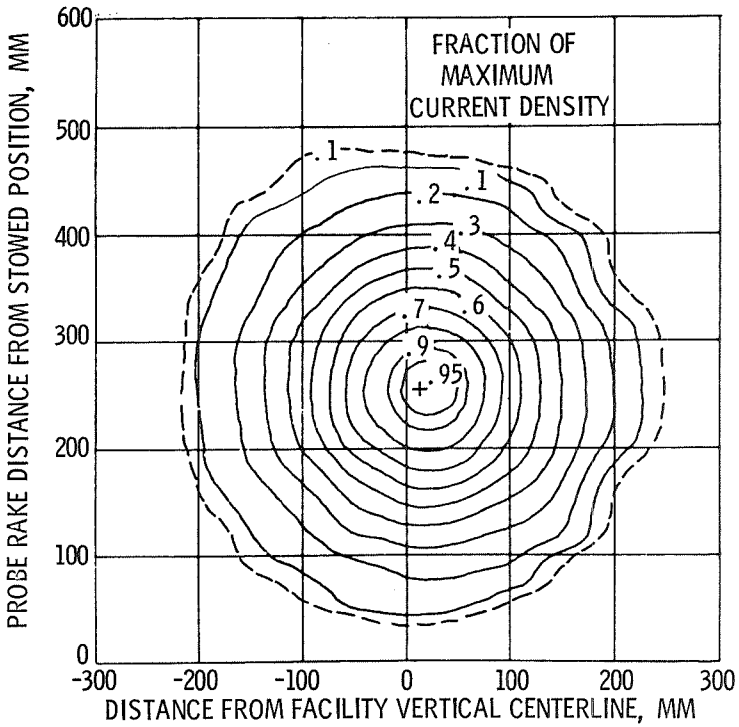

Figure 10. - Beam current density contour map taken with punched molybdenum grid shown in figure 8 at 600 net accelerating voltage. Dash curve from 450 volt point.

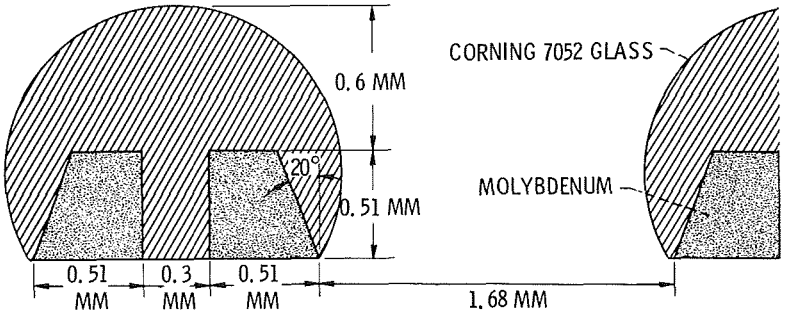

Figure 11. - Cross-sectional geometry of typical element set of glass coated electric discharge machined quadrant vector grid.

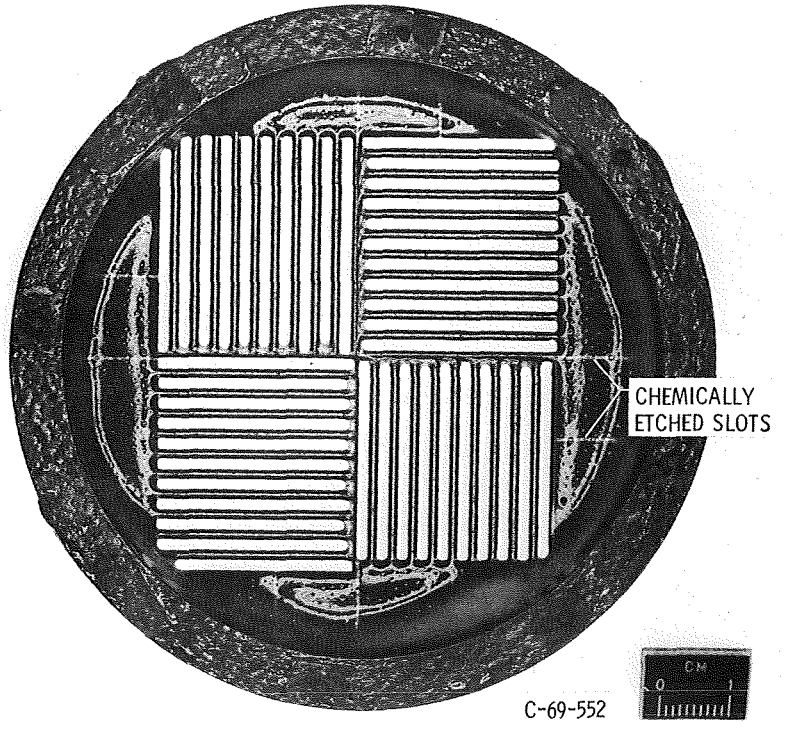

Figure 12. - Coated side of quadrant vector grid showing peripheral support ring.

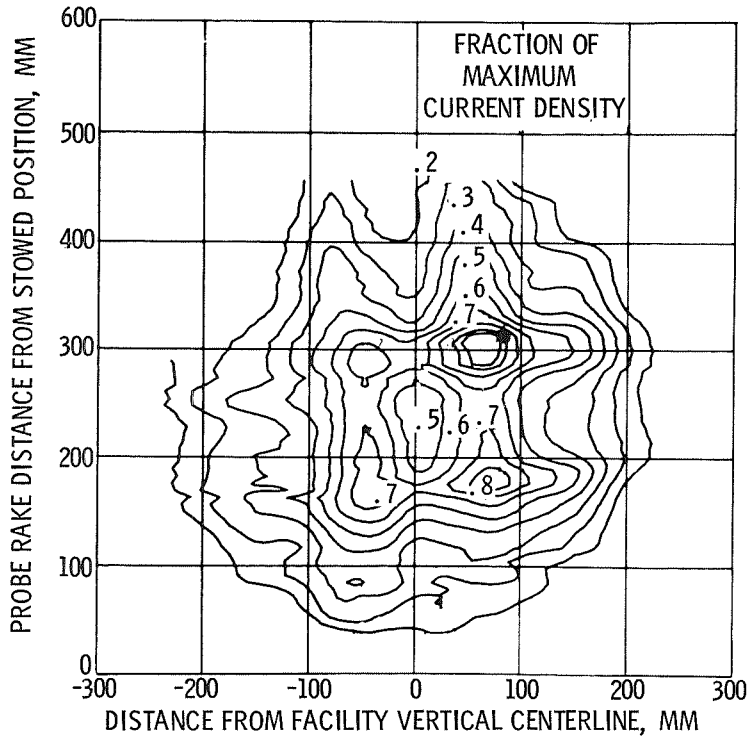

Figure 13. - Beam current density contour map taken with quadrant vector grid at 200 volts net accelerating potential and a 6.6 mA beam current.

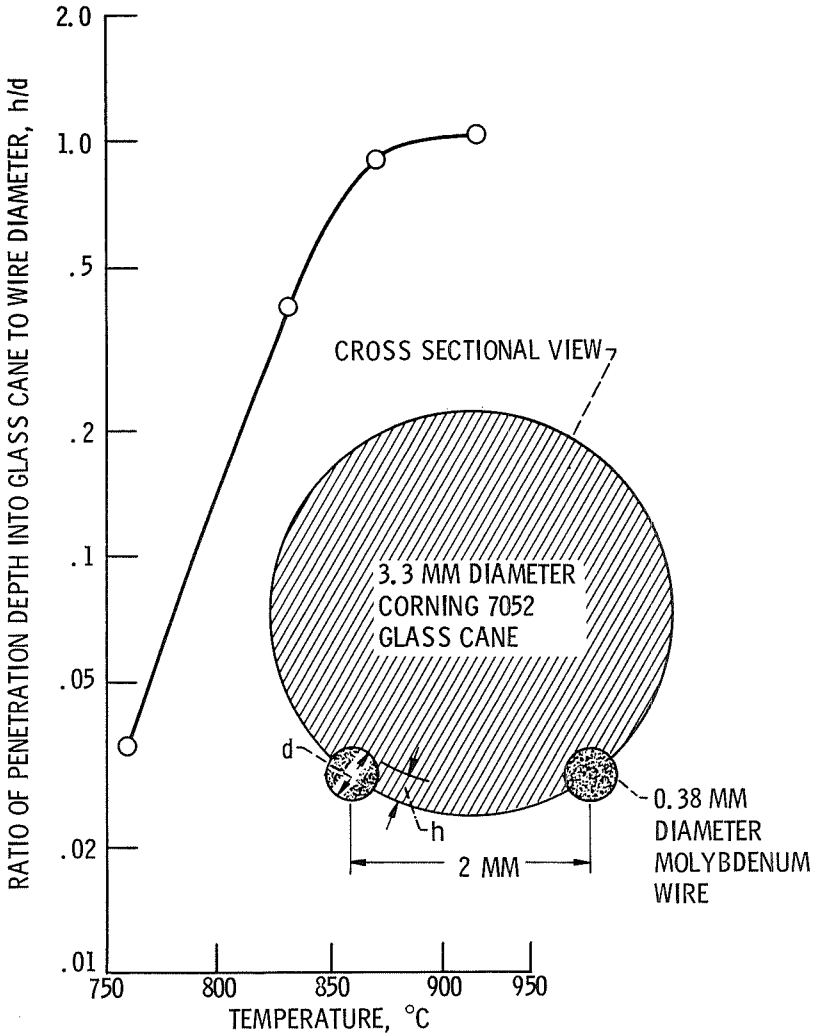

Figure 14. - Ratio of penetration depth into glass cone as a function of temperature for a 1 hour heating period.

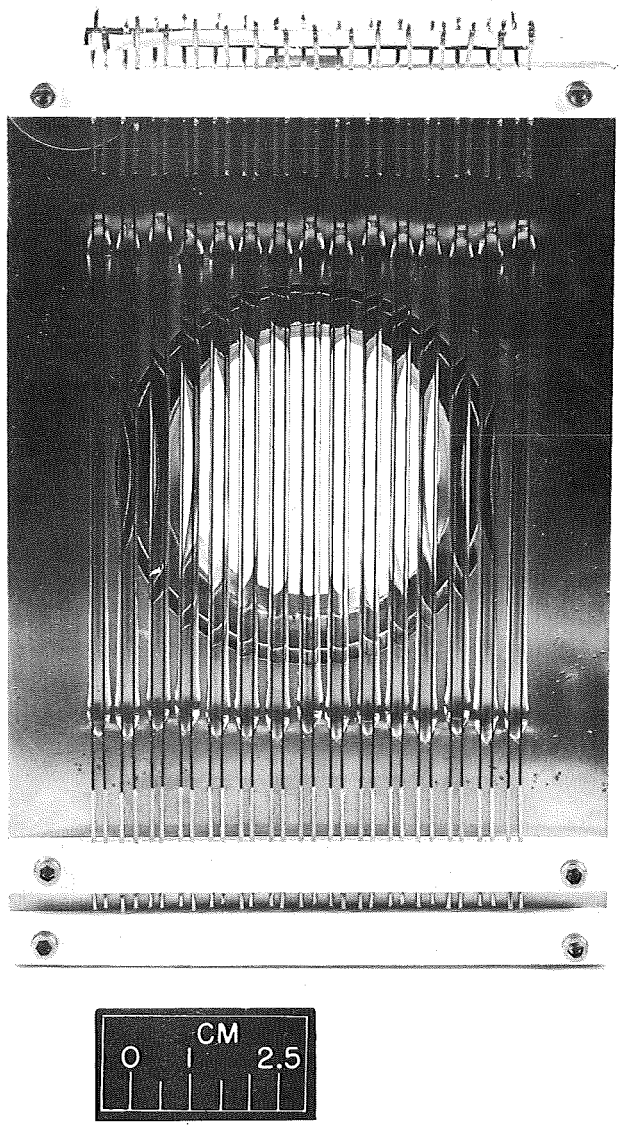

C-69-1265

Figure 15. - Glass cane and parallel wire composite grid for 5 cm diameter thruster.

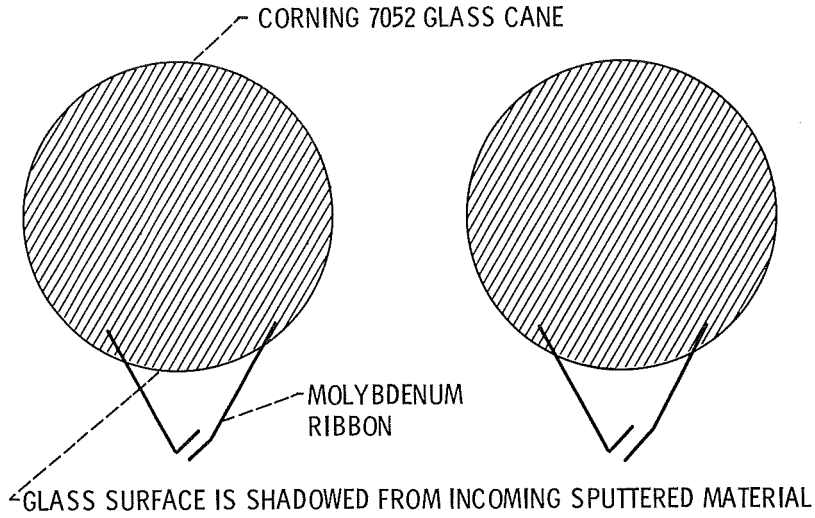

Figure 16. - Cross section of shadow shielded vector grid concept.

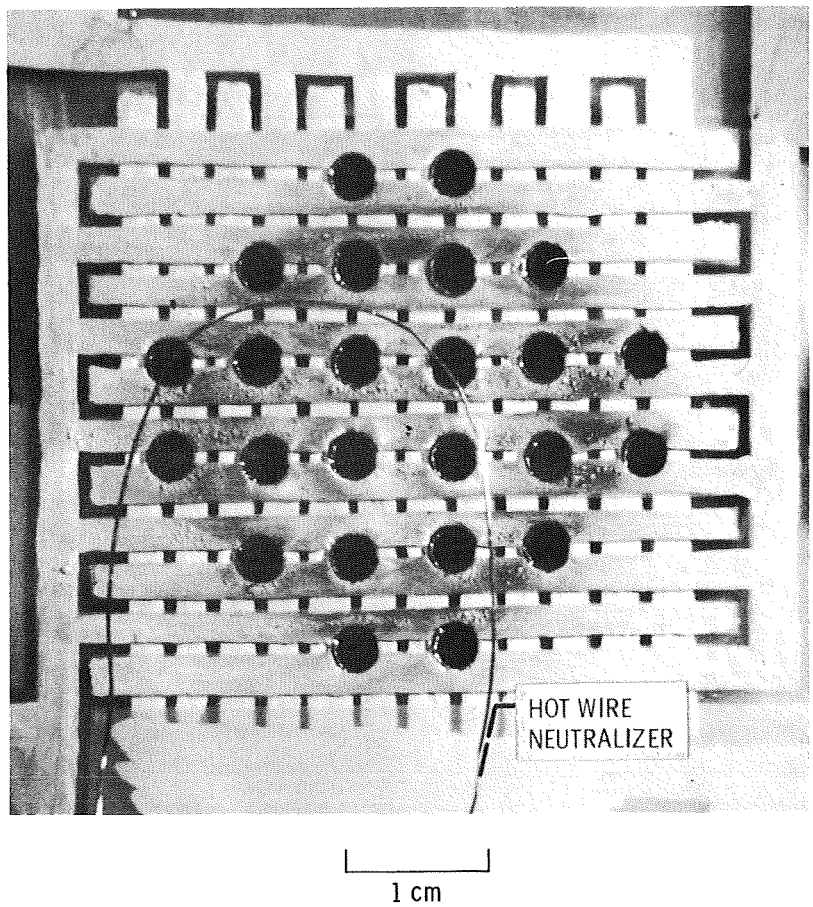

Figure 17. - Downstream surface of laminated grid. Apertures 3 mm diameter.

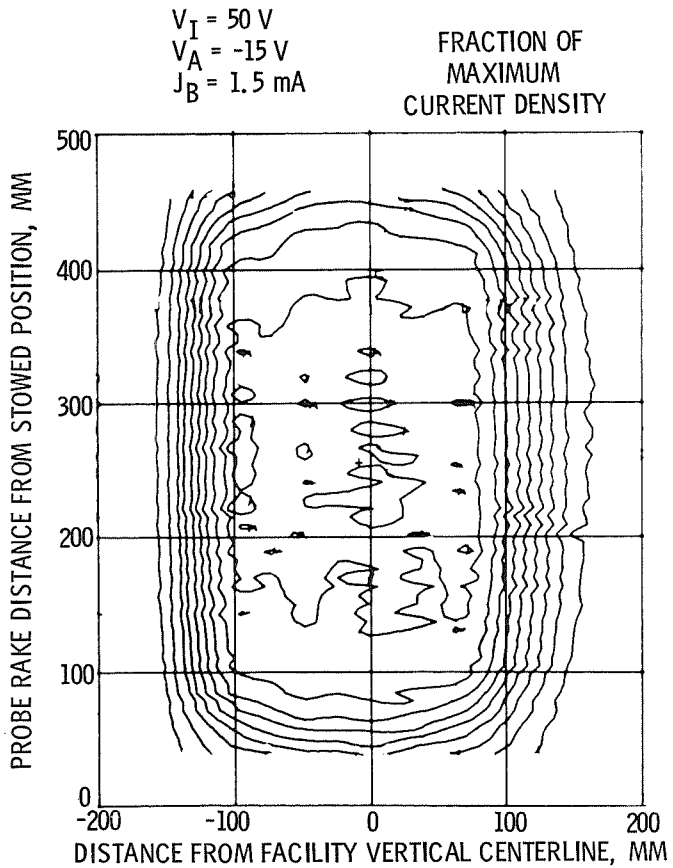

Figure 18. - Beam current density contour map with laminated composite grid.

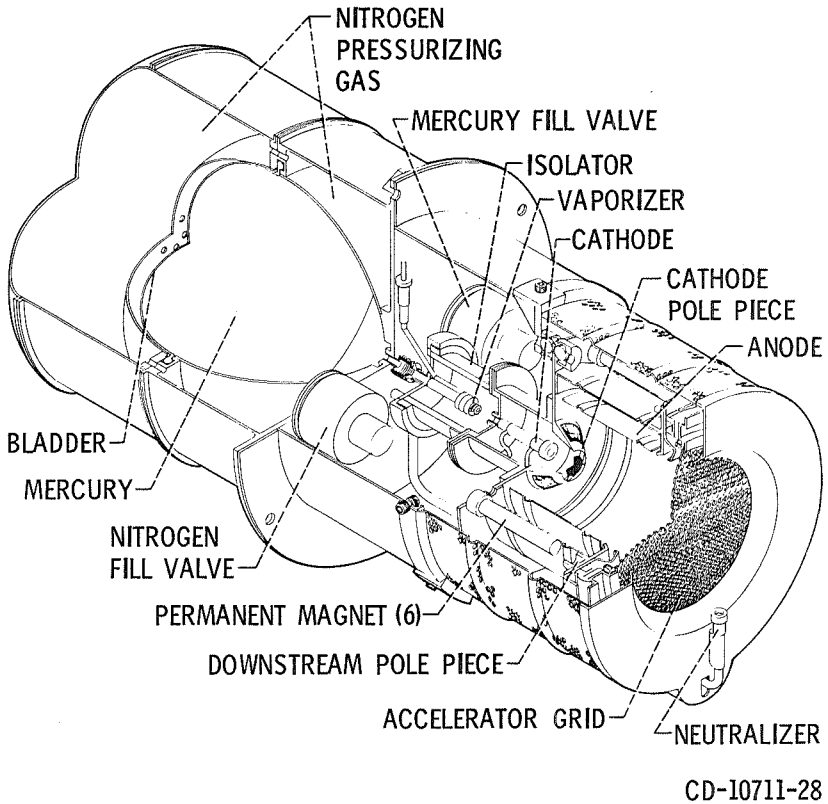

Figure 19. - 5-cm electron-bombardment thruster system.